Communication

# High-performance 3D tubular nanomembrane sensor for DNA detection

Mariana Medina-Sánchez, Bergoi Ibarlucea, Nicolas Pérez, Dmitriy D. Karnaushenko, Sonja M. Weiz, Larysa Baraban, Gianaurelio Cuniberti, and Oliver G. Schmidt

*Nano Lett.*, **Just Accepted Manuscript** • DOI: 10.1021/acs.nanolett.6b01337 • Publication Date (Web): 06 Jun 2016

# High-performance 3D tubular nanomembrane sensor for DNA detection

*Mariana Medina-Sánchez[1*], Bergoi Ibarlucea[2*], Nicolás Pérez [1], Dmitriy D. Karnaushenko [1], Sonja M. Weiz [1], Larysa Baraban[2], Gianaurelio Cuniberti[2], Oliver G. Schmidt[1,3]*

*[1]Institute for Integrative Nanosciences, IFW Dresden, Helmholtzstraße 20, 01069 Dresden, Germany*

*[2] Institute of Materials Science and Max Bergmann Center for Biomaterials, Center for Advancing Electronics Dresden (CfAED), Dresden University of Technology, 01062 Dresden, Germany*

*[3]Material Systems for Nanoelectronics, Chemnitz University of Technology, Reichenhainer Straße 70, 09107 Chemnitz, Germany*

ABSTRACT

We report an ultrasensitive label-free DNA biosensor with fully on-chip integrated rolled-up nanomembrane electrodes, in which the hybridization of complementary DNA strands (Avian Influenza Virus subtype H1N1) is selectively detected down to attomolar concentrations - an unprecedented level for miniaturized sensors without amplification. Impedimetric DNA detection with such a rolled-up biosensor shows four orders of magnitude sensitivity improvement over its planar counterpart. Furthermore, it is observed that the impedance response of the proposed device is contrary to the expected behavior due to its particular geometry. To further investigate this difference, a thorough model analysis of the measured signal and the electric field calculation was performed, revealing enhanced electron hopping/tunneling along the DNA chains due to an enriched electric field inside the tube. Likewise, conformational changes of DNA might also contribute to this effect. Accordingly, these highly integrated three-dimensional sensors provide a tool to study electrical properties of DNA under versatile experimental conditions and open a new avenue for novel biosensing applications (i.e. for protein, enzyme detection or monitoring of cell behavior under in-vivo like conditions).

KEYWORDS: DNA biosensor, electrochemical impedance spectroscopy, H1N1 Avian Influenza Virus, rolled-up nanotechnology, tubular electrodes.

## Introduction

Advances in genomics over the past decades have made the hybridization of complementary DNA chains a crucial tool for the recognition and monitoring of sequences belonging to infectious diseases.[1] DNA of Avian Influenza A virus (AIV), subtype H1N1, is an analyte of important interest due to its pandemic recurrence.[2,3] Standardized methods for detection and identification of influenza viruses are normally used. They involve complex and time-consuming processes as for example virus isolation in cell culture or in fertilized chicken eggs, haemagglutination inhibition testing, immunofluorescence sensing, antigen tests, or DNA amplification by using polymerase chain reaction (PCR).[4] The PCR technique is most commonly used due to its high sensitivity and rapid performance, coupled to a prior reverse transcription step to obtain the complementary DNA (cDNA) from the virus' RNA. However, in order to avoid transcription errors during the amplification process, it is preferable to use direct DNA detection, as is the case of the biosensor proposed in this work.

Other methods, well-suited for point-of-care applications, such as biosensors based on silicon nanowire field-effect transistors,[5] DNA microarrays [6] or electrochemical sensors,[7] have also been reported in the literature. These methods need the use of auxiliary labels, nanomaterials, or amplification strategies,[8] and the demonstrated detection limits remain in the pico- or femtomolar range, not as good as the one communicated in our work.

Among the aforementioned detection techniques, electrochemical impedance spectroscopy (EIS)[9] is gaining attention for DNA determination in solution due to its high sensitivity and label-free nature.[10,11] Here, the hybridization itself can be directly quantified in relation to the

resistance offered to the electron transfer for the reduction/oxidation (redox) reaction of a mediator. The evolution of the redox reaction is then probed by monitoring the linearity of the voltage-current response in a range of frequencies and fitting the results using an equivalent circuit model.[12] In comparison, fluorescence-based DNA detection systems[13–15] use indirect quantification methods that require more complex procedures as well as more expensive instrumentation and reagents.[16] Compared to other electrochemical techniques, EIS is not destructive for the biomolecules and allows separating the surface binding events from the ones in the bulk solution. Additionally, it offers a higher sensitivity when the concentration of the target analyte and the current level changes are small due to the inverse relation of impedance with conductivity.[17]

Moreover, microelectronics and microfabrication processes make EIS-based devices easy to miniaturize and integrate, allowing a lab-on-a-chip type detection, which presents advantages in portability, low reagent consumption, and reduced cost of instrumentation.[18] The applicability of the technique for DNA detection in miniaturized devices has been previously demonstrated for different sequences but with limitations in either sensitivity, [19,20] reagent and sample consumption[21] or suitability for device integration.[22]

Many efforts have been dedicated to the development of novel electrode configurations that can be integrated in microfluidic platforms to create miniaturized transducers. The enhancement of sensitivity in such devices has been achieved, for example, by increasing the sensing area with porous surfaces,[23] decreasing stray capacitances,[24] modifying the surfaces with conductive nanomaterials, or using electrical/electrochemical labels.[25] Different approaches for integrated electrode fabrication have been reported: sidewall transducers utilizing low melting point metal alloys,[26] water-assisted femtosecond-laser ablation followed by electroless plating,[27] semicircular

electrodes,[28] top-bottom electrochemical electrodes,[29] and porous materials integrated in electric transducers.[14] Nevertheless, such approaches present some inherent drawbacks such as material availability limitation, reusability restrictions, and long inter-electrode distance leading to only average detection limits in the top-bottom electrochemical configuration or lack of demonstration as biosensors in some of the cases.

More recently, microtubular devices fabricated by rolled-up nanotechnology[30] have been used for the fabrication of fully integrated optofluidic resonators,[31] capacitors,[32] batteries,[33,34], antennas[35] and field-effect transistors.[36,37] Lately, a rolled-up conductimetric sensor reported by Martinez-Cisneros et al.[38] showed an improvement in performance of two orders of magnitude compared to conventional planar electrodes when different ionic species were detected. A single-cell resolution was also demonstrated using such sensor, opening new possibilities for lab-in-a-tube biosensing platforms.[39,40] However, the behavior of rolled-up tubes upon incorporation of a biorecognition element and exposure to a target analyte in order to study their performance as biosensor is unknown.

Here, we develop the first biosensor based on fully integrated rolled-up microelectrodes[30] for ultra-sensitive DNA detection without using any label or amplification strategy, or requiring additional materials to increase the performance. The work includes a microscale impedimetric transduction setup (**Figure 1a**). The electrodes are prepared via sequential deposition of strained nanomembranes onto a sacrificial layer that is then selectively dissolved, resulting in the self-roll-up of the microtubular electrodes. The obtained impedimetric signal after DNA hybridization is compared to the one found using planar geometry. The planar electrode configuration attains picomolar detection of H1N1 AIV DNA, whereas in the rolled-up configuration, attomolar concentrations are detected at four-fold lower noise levels. Additionally,

no unspecific response is observed when the DNA-functionalized tubular electrodes are exposed to the non-complementary sequences of H5N1 subtype DNA. Such result would allow full integration into lab-on-a-chip devices for direct detection after reverse transcription of the virus RNA, saving processing time and cost. Hence, our platform offers the possibility to study DNA conductivity properties as well as the hybridization event in a direct way, using very low DNA concentration, as for the first time a clear increase in the conductivity is observed and discussed when the DNA concentration rises, in sharp contrast to the reported planar devices.

## Results

### *Electrode fabrication and characterization*

The fabrication process of rolled-up electrodes, based on sequential deposition of strained multilayer nanomembranes on a sacrificial layer that was later selectively etched (**Figure 1b)**, resulted in tubular electrodes of approximately 1.2 windings, 220 μm in length, and about 28.5 μm in diameter, with fingers width of 10 μm and interdigital distance of 5 μm. Their encapsulation in a microfluidic device allows the integration as a linear array on a single chip (**Figure 1c-g).** More details of the fabrication procedure can be found in the experimental part.

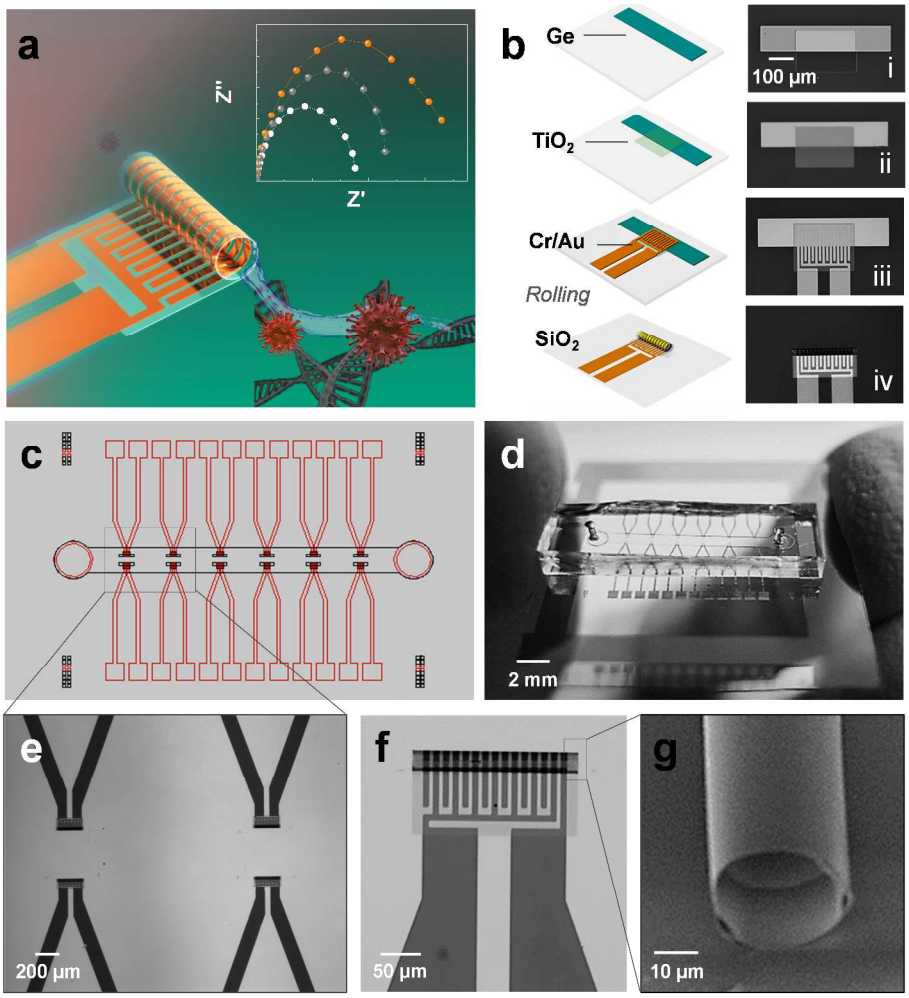


**Figure 1.** (a) General concept of the proposed work, showing viral genetic information entering the microelectrodes and showing impedance changes. (b) Steps for the fabrication of tubular electrodes: i) Ge ii) strained $TiO_2$ bilayer iii) Cr/Au and iv) $SiO_2$ passivation layer. (c) Layout of the electrode and fluidic design. (d) Final fabricated device. (e) View of the tubular electrodes inside the fluidic channel. (f) Single tubular electrode and (g) its scanning electron microscope image.

Initial characterization of the bare electrodes using cyclic voltammetry (**Figure 2a and 2b**, and **Figure S1**) clearly showed a more linear response and lower limit of detection (LOD) in the tubular electrodes compared to the planar counterparts. This limit of detection was calculated following the 3σ/slope criterion[41] of the International Union of Pure and Applied Chemistry

(IUPAC). LOD of the rolled-up configuration in the presence of ferricyanide along the whole measured range (0.016 to 10 mM) is about 0.37±0.01 mM compared to 1.7±0.2 mM for the planar geometry (0.32 to 10 mM range).

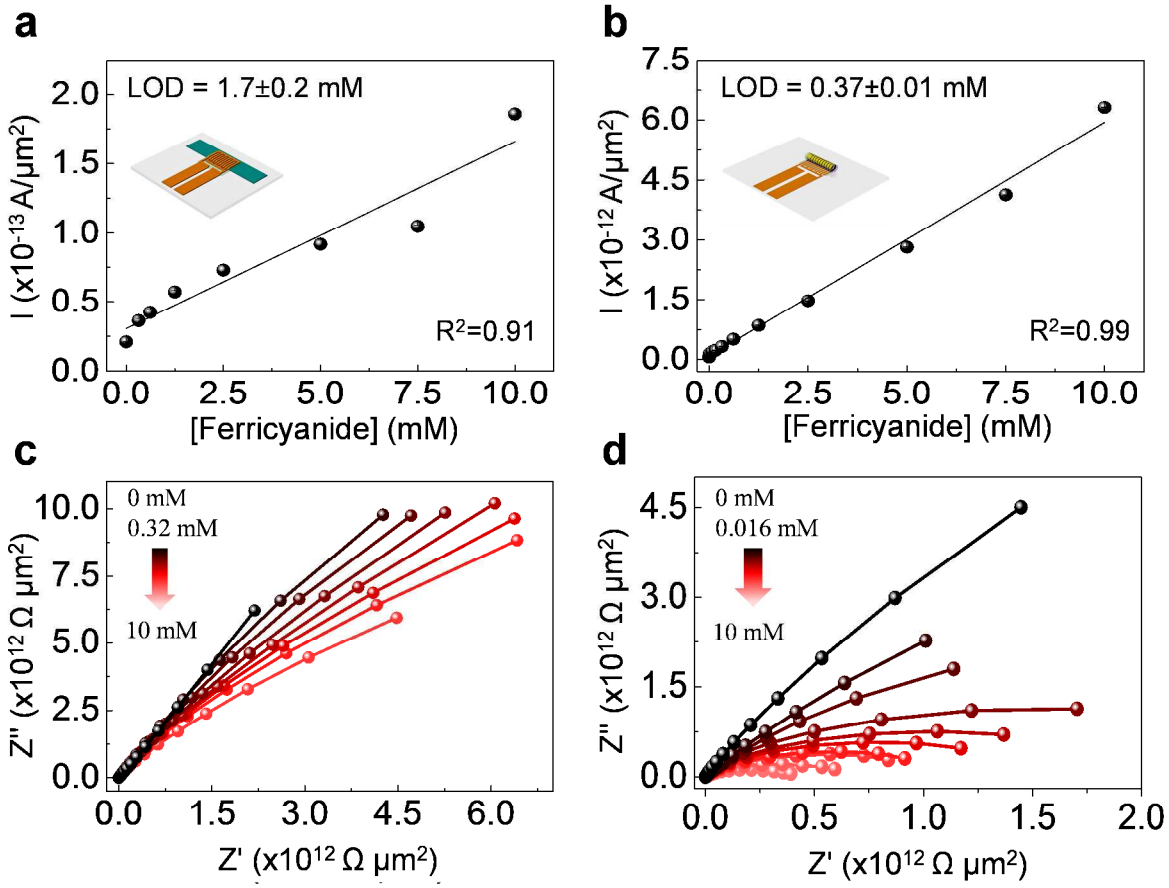


**Figure 2.** Characterization of unmodified electrodes with ferricyanide: calibration by cyclic voltammetry on (a) planar and (b) tubular electrodes at 0.5 V. Impedance measurements on (c) planar and (d) tubular electrodes.

The same concentration range was measured by EIS (**Figure 2c and 2d**) and showed a good reproducibility as seen in **Figure S1b inset** for three repeated measurements of 10 mM ferricyanide with different electrodes, the redox probe concentration for further DNA detection.

*Characterization of the biofunctionalization*

The biofunctionalization process (**Figure 3a**) was first monitored on planar surfaces by contact angle and XPS measurements. The contact angle values after each modification step can be seen as inset microphotographs in **Figure 3b**. Bare gold showed a contact angle value of 74˚. After the incorporation of 11-mercaptoundecanoic acid (11-MUA), it decreased to 33˚, a similar value to the one reported for other surfaces that also present exposed carboxylic groups.[42] There was a further decrease to 25˚ after the oligonucleotide immobilization, keeping the surface hydrophilic as expected.[43]

Impedance measurements were additionally performed after each modification step of the electrodes (**Figure 3b**). The impedance signal showed a significant change after the 11-MUA attachment and oligonucleotide immobilization. However, when the carboxylic group of 11-MUA was not activated with EDC and NHS, the incubation with the oligonucleotide did not produce any difference, showing that there was no adsorption of the DNA probe.

This surface modification significantly affects the interaction between the redox probe and the electrode surface (**Figure 3c**), as the hybridization event can be directly measured in relation to the resistance offered to the electron transfer for the reduction/oxidation (redox) reaction of a mediator.

Additionally, the X-Ray Photoelectron Spectroscopy (XPS) study also indicated a successful surface modification. **Table S1 (SI)** shows the atom content in percentage extracted from the XPS survey scan. This content varied accordingly to the specific composition of the new layers after each modification step. High resolution spectra of the C1s (**Figure S2a**), S2p (**Figure S2b**), N1s (**Figure S3a**) and P2p (**Figure S3b**) regions were also recorded, showing the presence of the

specific peaks belonging to each new bond. More details on the XPS study can be found in the **SI**.

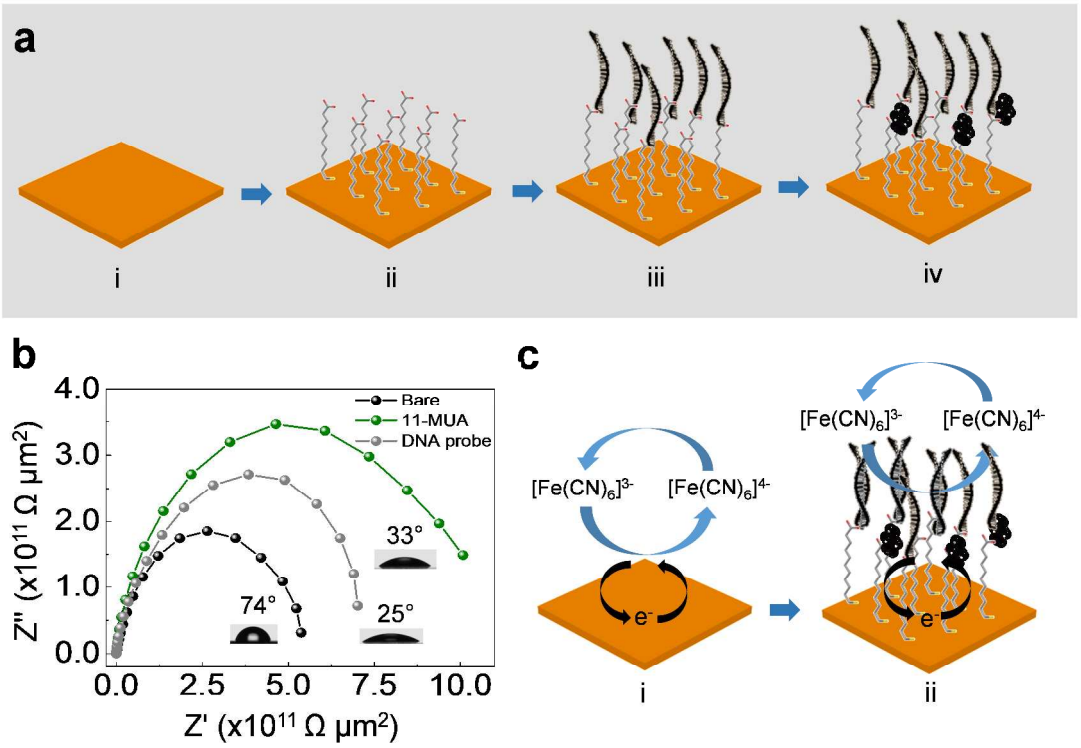


**Figure 3.** (a) Biofunctionalization steps: i) bare gold, ii) 11-MUA SAM formation, iii) DNA probe immobilization, and iv) blocking of remaining carboxylic groups with ethanolamine. (b) Impedance and water contact angle values for the different resulting surfaces after each modification step. (c) Principles of EIS measurement. Charge transfer occurs between the redox probe and the electrode, which is affected by the organic layer in between.

*Biosensor response*

During the study of the biosensing response, the opposite tendency was observed in the EIS data between planar and tubular electrodes when the target DNA was incubated. For the planar electrodes impedance values increase with increasing DNA concentration, whereas for the rolled-up electrodes impedance values decrease. This can be clearly seen in the frequency sweep

in presence of $[Fe(CN)_6]^{3-}$ (**Figure 4a and 4b**) and in the chronoimpedance tests (**Figure S4**). It was also evident that for the planar electrodes a significant increase in the impedance occurred only at 200 pM DNA concentration remaining almost unchanged for lower values. For the rolled-up electrodes, on the contrary, a gradual and significant reduction of the impedance was observed for DNA concentrations ranging from 20 aM to 2 pM. It is worth noting that the tubular configuration is very efficient in cancelling the external noise and enables accurate measurement of the impedance with a noise level by a factor of four lower than that of the planar electrodes. An RMS of 1.8 Ω was measured for the tubular configuration, and 7.6 Ω for the planar electrodes (**Figure S4**).

Few recent publications have demonstrated biosensors with high sensitivity, comparable to that presented in our work. Unlike ours, these methods required DNA amplification by using PCR, the use of additional nanomaterials to enhance the sensitivity or more complex equipment, making them not suitable for point of care or miniaturized analytical devices. In our work, therefore, simplicity is gained in sample handling and signal read out. To better illustrate this breakthrough, **Table 1** summarizes cutting edge research on DNA biosensing and compares it to our work. All in all, this evidences the efforts of the community in looking for strategies to improve the sensitivity of current technologies and the development of new setups that combine portability and high-performance sensors. Our approach can satisfy all of these requirements, showing a very good performance in a microliter sample range, and no need of additional labeling or amplification strategies. Additionally, it is suitable for massive parallel monolithic on-chip integration. However, this does not mean that it is incompatible with other nanomaterials and measurement processes that would open new detection possibilities, especially when the analyte is not easily detectable.

In order to gain insight into the response of the electrodes, they were modeled using a widely accepted equivalent circuit for the behavior of metallic electrodes covered with organic material.[44] The equivalent circuit (**Figure 4c**) contains a minimum number of parameters that can be correlated to actual features of the systems studied in this work. Namely, solution resistance ($R_S$), resistance in the areas not fully covered with organic material ($R_{HOLE}$), charge transfer resistance ($R_{CT}$), constant phase elements accounting for capacitance effects due to the organic coating ($Q_C$), the double layer ($Q_{DL}$), and finally a Warburg term, analogous to a capacitance, accounting for diffusion limited charge transport in the solution (W). The fitted curves reproduced the impedance data with accuracy better than 98% in all cases (**Figure S5**). The results of the fitting show that for the rolled-up electrodes, $R_{HOLE}$ (**Figure S5a**) and, especially, $R_{CT}$ are very sensitive to the variation of the DNA concentration in the aM - pM range compared to the pM range observed for the planar electrodes (**Figure 4d**). The capacitances associated with the double layer show also a significant variation with DNA concentration in the rolled-up electrodes (**Figure S5b and S5c**).

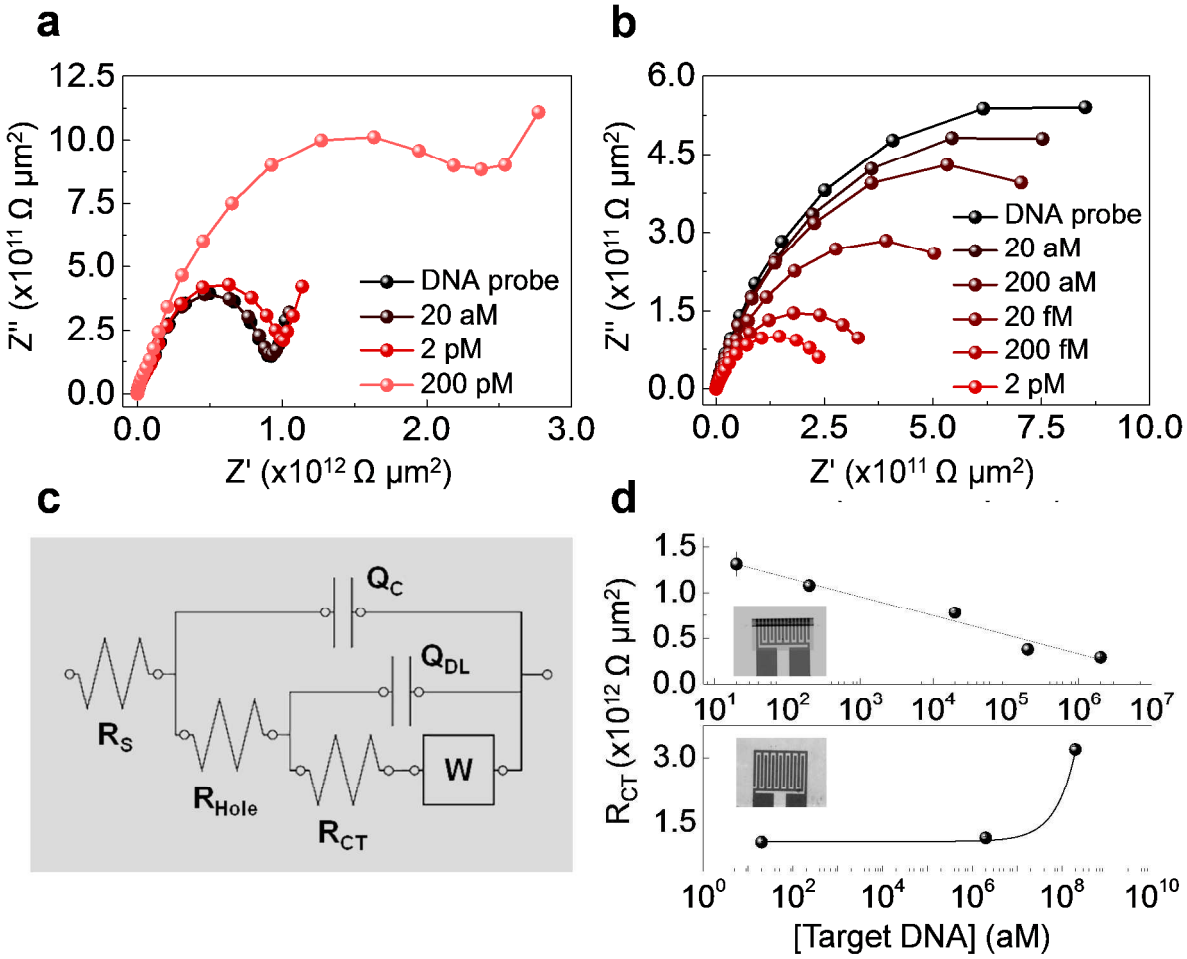


**Figure 4.** Impedance measurements after different target DNA hybridizations (a) on planar and (b) tubular electrodes, (c) equivalent circuit considered for the fitting of the Nyquist plots for both configurations, and (d) plots of $R_{CT}$ of the resulting semicircles in the Nyquist plots.

**Table 1.** Summarizing table comparing recent research on DNA biosensing.

| Technique | Nanomaterial/amplification | LOD | Volume | Integration level |
|---|---|---|---|---|
| Surface plasmon resonance[45] | Nanorods assembled by DNA bridges/PCR | 3.7 aM | 100 µL – 25 mL (including primers and amplification solutions) | -- |
| Mass spectroscopy[46] | Cr/Au coated piezoelectric plate sensors | 1.6 aM | 55 mL | -- |
| Linear stripping voltammetry [47] | Gold nanoparticle amplification<br>*(Bulk electrodes ➔ WE: Au, CE: Pt, RE: Ag/AgCl )* | fM | 100 µL | -- |
| EIS[8] | Sandwich scheme with gold nanoparticle amplification<br>*(Screen printed carbon electrode modified with carbon nanotubes)* | 577 pM | 13 µL | -- |
| EIS[9] | Adjunt probe for amplification<br>*(Bulk electrodes ➔ WE: Au, CE: Pt, RE: Ag/AgCl )* | 6.3 pM | 30 µL | -- |
| EIS[48] | Enzymatic recycling + gold nanoparticle amplification<br>*(Bulk electrodes ➔ WE: Au, CE: Pt, RE: calomel )* | 0.6 pM | 20 µL | -- |
| EIS[11] | No special materials/amplification<br>*(Planar microelectrodes ➔ Pt)* | 10 nM | Not mentioned (µL range) | ++ |
| EIS[49] | Polyaniline/polyacrylate (PANI/PAA) electropolymerization on electrodes<br>*(Bulk electrodes ➔ Boron doped diamond electrodes)* | 20 nM | 25 µL | -- |
| EIS[50] | Poly(p-phenylene) PPP modified with ferrocene groups<br>*(Bulk electrodes ➔ WE: Au, CE: Pt, RE: Ag/AgCl )* | 30 fM | Not mentioned | -- |
| Square-wave voltammetry[51] | Copper complex and graphene modified glassy carbon electrode | 0.199 pM | Not mentioned | -- |
| EIS[52] | Polyaniline-molybdenum disulfide (PANI-MoS2) nanocomposite<br>*(Bulk electrodes ➔ WE: carbon paste, CE: Pt and RE: saturated calomel electrode)* | 200 aM | 20 µL | -- |
| EIS[53] | Gold nanoparticle amplification<br>*(Bulk electrodes ➔ WE: gold, CE: Pt and RE: Ag/AgCl)* | 0.3 fM | Not mentioned | -- |

| | | | | |
|---|---|---|---|---|
| EIS[54] | Poly(indole-5-carboxylic acid) electropolymerized on ZnO<br><br>*(Bulk electrodes ➔ WE: carbon paste, CE: Pt, and RE: saturated calomel)* | 220 aM | 10 µL | -- |
| EIS[22] | Graphene and carbon nanotubes modified glassy carbon electrodes<br><br>*(Bulk electrodes ➔ WE: glassy carbon, CE: Pt and RE: Ag/AgCl)* | Lower LOD<br><br>0.35 aM | mL range | -- |
| EIS[55] | Graphene nanosheets modified *(Bulk electrodes ➔ WE: glassy carbon, CE: Pt and RE: Ag/AgCl)* | 7.1 zM | mL range | -- |
| Our (EIS) | No special materials/amplification<br><br>*(Rolled-up microelectrodes ➔ Au)* | 20 aM | 25 µL | ++ |

* EIS: Electrochemical impedance spectroscopy. ++ Monolithic on-chip integration. WE: Working electrode. CE: Counter electrode. RE: Reference electrode.

It can be concluded that the major impact on the change of impedance with DNA concentration originates from the variation in $R_{CT}$. The hybridization of DNA, which has a negative charge polarization at the phosphate groups of the backbone, is expected to repel the redox probe due to electrostatic effects and thus increase $R_{CT}$ in conventional co-planar electrodes,[12] which is also observed in the present case (**Figure 4d**). For the rolled-up electrodes, $R_{CT}$ decreases semi-logarithmically with increasing DNA concentration up to the measured limit of 2 pM (**Figure 4d**). Incubation with only the hybridization buffer solution showed no change (**Figure S6**), indicating that the striking differences are due to hybridization and not due to salt deposition, electrode degradation, or removal of the biofunctionalization layer.

In order to understand the possible influence of electrode geometry, the electric field distribution was calculated using a finite elements model for both electrode types, considering they were immersed in water with conductivity 0.2 µS/m. The simulation shows that the rolled-up

geometry generates a higher field inside the tube than the one generated by the planar electrode in an equivalent volume above the bottom of the channel (**Figure 5**). For the rolled-up electrode the mean value of electric field calculated over a cross section of the tube is $5.1x10^4$ V/m, whereas in the same cross section over a planar electrode it is $1.8x10^4$ V/m (see **Figure 5a**). **Figure 5b** shows the profile of the field values at increasing distance from the bottom of the channel (gray arrow). The edges of the tube can be clearly identified by the high electric field values. Remarkably, at the center of the rolled-up electrodes (marked with a white dashed line in **Figure 5b**), the values obtained are considerably higher than for the planar electrode at the same distance.

Sections with overlapping windings may be found in rolled-up electrodes (red arrow in **Figure 5a**). Calculated electric field values in the middle of a 2 μm spacing between such overlapping sections may reach up to $4.7x10^5$ V/m at certain positions along the tube. The relative relevance in the measurements of these locally very high field values in the overlapping parts needs to be further investigated in future studies.

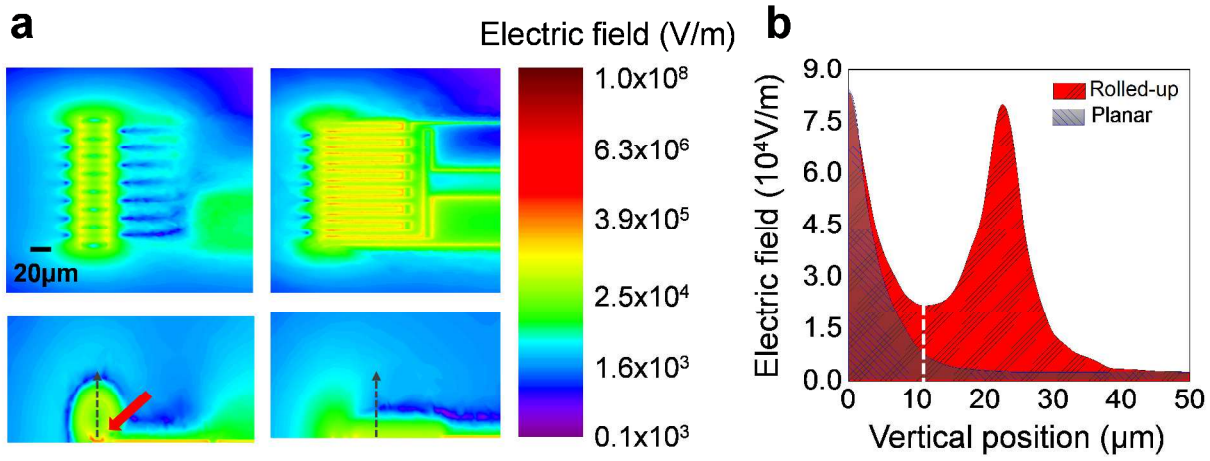


**Figure 5.** Amplitude of the electric field for a planar and a rolled-up electrode calculated for a sinusoidal driving voltage of amplitude 0.35 V and frequency 100 kHz. (a) Intensity map of the electric field generated by the tubular electrode and the planar electrode. Red arrow indicates area of overlapping windings. (b) Transverse profile of the average electric field of a cross-section in the direction of the grey dashed arrows in the 2d color maps. White dashed line indicates the position corresponding to the center of the tube.

The calculation shows that the rolled-up geometry is more efficient in deploying higher fields but, more importantly, in uniformly distributing that high field through the bulk of the electrolyte. This implies a higher drift velocity of ions in the solution and so, $[Fe(CN)_6]^{3-}$ ion migration towards the electrode is enhanced. Additionally, for timescales such as in our experiments at low frequencies, the typical thickness of the depletion layer for ferricyanide in aqueous solution is of the order of some microns[56] which is of the order of the rolled-up electrode radius. This is consistent with the negligible Warburg contribution obtained in the fitting (**Figure S5d**). On the contrary, for the planar electrodes diffusion limited transport has a relevant contribution to the total impedance (**Figure S5d**) rendering the electrodes less sensitive to DNA concentration changes.

On the other hand, the cyclic voltammetry in **Figure S1a and S1b** shows an increased current in the rolled-up electrodes. This implies an increased double layer capacitance of the bare rolled-up electrodes compared to the planar ones **(Figure S1c)**. The fitting of the impedance measurements also indicate increased double layer capacitance in the rolled-up electrodes (**Figure S5c**). The larger charge accumulation at the rolled-up electrode's surface would then be drained by hopping/tunneling along the DNA chains,[57–59] which would lead to the observed reduction in $R_{CT}$ with increased DNA concentration. Double-stranded DNA has significant electronic conductivity due to the base pair stacking, unlike single-stranded DNA.[60,61] However, its conductivity also depends on many parameters such as the sequence, length, environment, microstructures, interfaces, preparation and detection protocol.[62] It can also be affected by external electric fields.[63,64] This transport occurs either by incoherent hopping or coherent tunneling through neighboring DNA base pairs, reaching the ferricyanide molecules for the redox reaction (**Figure S7a**). The ability of DNA to transfer electrons from a gold electrode to a redox probe was already demonstrated for helices of up to 100 base pairs.[65]

On the contrary, planar electrodes show depletion layer effects, resulting in no sensitivity at low DNA concentrations. Only at very high DNA concentrations an increase of impedance is detected. The reduction in the coating capacitance obtained in the fitting indicates that, in that case, DNA acts just as dielectric barrier that keeps the charges away from the electrode.

Taking into account all of our findings, we propose that in the rolled-up geometry, the increase in the electric field at distances corresponding to the typical depletion layer thickness of ferricyanide favors ionic migration, effectively suppressing the depletion layer effect. Combined with the ability of the rolled-up electrodes to accumulate charge at its surface, this makes the charge transfer via conduction through double stranded DNA much more efficient that for the

planar electrodes. In that latter case the variation in impedance would arise because of the building up of a dielectric barrier, which can be noticed only at higher DNA concentrations. In this way the opposite behavior of the impedance and the higher sensitivity of the rolled-up electrodes can be explained.

A second explanation of the opposite behavior in the two geometries, based on conformational changes, cannot be discarded. It has been shown that under strong enough electric fields (hundreds of volts per centimeter), ssDNA undergoes isotropic compression. Upon hybridization, the equilibrium, non-compressed state, is restored.[66,67] Considering an initially applied high DC electric field on both electrodes to check their performance by cyclic voltammetry, the DNA is expected to compress.[67] The higher electric field value for the rolled-up electrodes produces strongly compressed DNA compared to the planar electrodes under the same applied voltage. After turning off the DC electric field, the DNA tends to recover its expanded form. Since the compression is higher for the RUE, DNA forms self-entangled structures, which find the expansion more difficult than for the planar electrodes. Therefore, more gold area remains covered by an organic insulating layer, as evidenced by a higher Rct (**Figure 4d).** Later, upon hybridization, an Rct increase occurs for planar electrodes as there is no further conformational change, only an addition of organic coating of the surface. On the contrary, in the RUE, the hybridized DNA expands liberating more gold surface, and in this way enabes electron transfer and decreasing the Rct. The graphical description of these steps is shown in **Figure S7b.**

Finally, the specificity of the biosensing response is demonstrated by incubation of different concentrations of the non-complementary sequence belonging to the AIV subtype H5N1, for which a low adsorption is observed after the first 20 aM. (**Figure S8**).

## Conclusions

In conclusion, the fabrication of a compact three-dimensional microtubular impedimetric biosensor with rolled-up nanotechnology fully integrated into microfluidic chips is presented. The tubular cavity was modified with capture DNA in order to selectively detect the AIV subtype H1N1. Tubular electrodes show enhanced performance in the aM-pM concentration range revealing an improvement of four orders of magnitude compared to planar configurations. The enhanced sensitivity would allow diluting real samples if necessary, reducing the noise produced by the presence of other biomolecules. The conductive behavior of DNA, on the other hand, would help to distinguish more easily the binding effect of the target analyte from the non-specific attachment of other biomolecules such as proteins. The last ones would insulate the electrodes, increasing the impedance signal, while the analyte hybridization would decrease it. This enhancement can be ascribed mainly to the variation of $R_{CT}$ and $Q_{DL}$ with increasing DNA concentration. Diffusion-limited transport is not relevant in the microtubular geometry. Specific detection of AIV H1N1 was achieved and discriminated from the H5N1 subtype. The observed reduction of $R_{CT}$ for the rolled-up electrodes, which is strikingly different to what is found for the planar ones, is consistent with enhanced electron hopping/tunneling along the DNA chains due to a higher electric field inside the tube compared to the planar feature. Conformational changes of DNA might also contribute to this effect.

The nanomembrane engineering used in the fabrication process sets the current biosensor apart from others previously reported in three key aspects: no additional labels or materials are needed, a very simplified measurement setup is sufficient, and just microliter sample volumes are

required, showing high integration level for point-of-care diagnostic platforms with minimum setup requirements.

Finally, this new geometry offers the potential to experimentally study electrical phenomena related to different DNA conformations (single or hybridized strands, mismatches or quadruplexes) that vary with the surface charge in tubular configurations, as well as electric field and impedimetric variables.

## Experimental Section

*Materials*

An e-beam deposition device was used with highest purity targets (99.7% for Ti, 99.95% for chromium and 99.99% for gold and $SiO_2$, and 99.5% for Germanium, Kurt J. Lesker, Jefferson Hills, PA, USA) for the fabrication of tubular electrodes. Photopatterning of the electrodes was performed using AZ5214 image reversal photoresist (Clariant, Frankfurt Am Main, Germany). Poly-dimethylsiloxane (PDMS) (SYLGARD 184, Dow Corning GmbH, Germany) and SU-8 negative tone resist (Microchem, Westborough, MA, USA) were used for the fabrication of microfluidic channels.

For the biofunctionalization procedures the following reagents were used: absolute ethanol, 11-mercaptoundecanoic acid (11-MUA), N-(3-Dimethylaminopropyl)-N'-ethylcarbodiimide hydrochloride (EDC), N-Hydroxysuccinimide (NHS), ethanolamine, phosphate buffered saline (PBS) in tablets, phosphate buffer (PB) and magnesium chloride ($MgCl_2$). The hybridization buffer used comprised 0.1 M Tris-HCl with 0.15 M NaCl and 20 mM $MgCl_2$ (pH 7). All reagents were purchased from Sigma-Aldrich and were used as supplied. All the oligonucleotides were ordered from Eurofins Genomics (Ebersberg, Germany). As analyte of interest, a specific

sequence of the AIV subtype H1N1 was used, with the sequence 5'-GTA GGT TGA CAG AGT GTG-3'. For its detection, a complementary sequence with an amino modification was used as DNA probe: 5'-$NH_2$-$(CH_2)_6$-CAC ACT CTG TCA ACC TAC-3'. As non-complementary target for the determination of subtype discrimination, a specific sequence of the AIV subtype H5N1 was used: 5'-TGA TAA CCA ATG CAG ATT TG-3'. Ferricyanide and phosphate buffer saline (Sigma Aldrich, Germany) was used as mediator for the electrochemical measurements.

*Fabrication*

The electrodes were fabricated using the self-rolling process of a strained multilayered nanomembrane (**Figure 1**), as reported elsewhere.[32] Briefly, a sacrificial layer (Ge 20 nm), a strained layer ($TiO_2$ 45 nm), and a bilayer for contacting (Cr 5 nm, Au 10 nm) were deposited in this order by e-beam evaporation onto a glass substrate (**Figure 1b**). Interdigitated electrodes were deposited on the strained layer using photolithography of AZ5214 photoresist. Finally, the sacrificial layer was dissolved using a solution of 5% (v/v) $H_2O_2$ in deionized water, leading to the rolling-up of the structure by strain relief of the underlying $TiO_2$. Mechanical stability and pad isolation were ensured by depositing 100 nm $SiO_2$ on top of the tubular electrodes, also with e-beam evaporation. By doing so, mainly the inner part of the tube would contact the work solution, although a small outer area might remain uninsulated due to the shadow effect of the circumference. An array of 12 electrodes was integrated into a microfluidic channel (**Figure 1c-e**) that was fabricated by soft-lithography as previously described.[68] In brief a four-inch silicon wafer was spin coated with a negative photoresist SU8-50 (Microchem, USA) and patterned by photolithography. Poly-dimethylsiloxane (PDMS) was poured onto the resulting mold and cured at 65 °C for 2 h. After this, the PDMS channel and glass substrate were assembled; both surfaces, glass containing the electrodes and PDMS, were activated for 30 s by oxygen plasma

(13.56 MHz/50W Generator, Diener Electronic GmbH + Co. KG, Ebhausen, Germany), and put into contact to achieve irreversible bonding. Final dimensions of the microfluidic channel were 500 μm width, 10 mm length and 50 μm depth. As indicated before, the obtained tubular electrodes with approximately 1.2 windings were 220 μm in length, ca. 28.5 μm in diameter, and had a fingers width of 10 μm and separation between them of 5 μm (**Figure 1f-g**). The continuous flow system set-up consisted of a set of syringes (neMESYS module, Cetoni GmbH, Korbußen, Germany) equipped with 0.4 mm internal diameter polyethylene tubing.

Planar interdigitated electrodes were also fabricated for comparison. Both geometries were characterized by repeated cyclic voltammetry and impedance measurements of a 1X PBS solution containing $[Fe(CN)_6]^{3-}$ in a concentration range from 0.016 mM to 10 mM. The behaviors of three different tubular electrodes were compared to each other to determine reproducibility. All measurements were normalized to the electrode active area. Electrochemical experiments were performed using an electrochemical analyzer μAutolab μ3AUT71270 (Metrohm Autolab B.V., Netherlands), which was connected to a personal computer using a software package GPS 4.9 (General Purpose Electrochemical System).

*Biofunctionalization*

The DNA probe for analyte detection was immobilized onto the gold electrodes following a protocol that involved a prior surface modification with thiolated molecules. Briefly, the electrodes were incubated overnight in absolute ethanol containing 10 mM 11-MUA. The loosely attached molecules were rinsed with ethanol. The sulfur atom of the thiol group in 11-MUA formed a strong dative bond with gold,[69] while leaving an exposed carboxylic group to which the amino-modified oligonucleotide could be attached. For this, the carboxylic groups

were activated by incubation for 15 min in 10 mM EDC and 5 mM NHS in 1X PBS buffer.[70] After rinsing with PBS, 20 μM amino-modified DNA, previously heated to 90 °C for 3 min and slowly cooled down to room temperature, was incubated in 1 M PB, in presence of 20 mM $MgCl_2$. The high buffer concentration helped to minimize the electrostatic repulsion between the phosphate backbones of the DNA molecules that would result in a low surface coverage,[71] while the $MgCl_2$ promoted the structural stability of DNA.[72] Then the electrodes were rinsed again with PB and a blocking step was carried out with 50 mM ethanolamine in hybridization buffer in order to block the possible remaining carboxylic groups and to minimize the physisorption of the analyte.[73] After a final rinse in hybridization buffer, the electrodes were ready to use.

The whole biofunctionalization procedure was monitored by contact angle (by deposition of 2 μL using an OCA Contact angle System from Dataphysics, Filderstadt, Germany) and X-ray Photoelectron Spectroscopy (XPS) measurements (using a PHI 5600 spectrometer with a monochromatic Al Kα 350W source, from Physical Electronics, Chanhassen, US) on planar surfaces and by impedance measurements directly on the microelectrodes.

*DNA detection*

Prior to the biosensing experiments, the target DNA sequence was heated to 90°C for 3 min and slowly cooled down to room temperature. Then it was diluted to the different target concentrations (20 aM to 200 pM) in hybridization buffer, and these were pumped into the microchannels. For each concentration, the flow was stopped and the sample was allowed to incubate on the electrodes for 20 minutes, followed by a rinsing with hybridization buffer to remove the DNA that did not hybridize. Finally, the measurement buffer (10 mM $[Fe(CN)_6]^{3-}$ in 1X PBS) was pumped and the resulting impedance of the electrodes was measured. The same

procedure was followed for the incubation with the non-complementary AIV subtype sequence in order to determine the specificity of the binding and to confirm AIV subtype discrimination. All measurements were normalized to the electrode active area.

EIS experiments were performed using the analyzer μAutolab μ3AUT71270, using a software package FRA 4.9 (Frequency Response Analysis system software). A frequency range from 0.1 Hz to 100 kHz was analyzed, using a sinusoidal AC potential of 0.35 V (rms).

*Finite elements simulation*

Finite element method (ANSYS Electromagnetics) was used to calculate the electric field distribution in the planar and the rolled-up structures. Dimensions of the real structure were defined as incoming parameters of the model. Only thicknesses of deposited layers were 10 times scaled-up and at the same time conductivity of metal layers were scaled-down in the same amount respectively to keep same normalized conductivity. Water was selected as media with a conductivity of 0.2 μS/m and relative permittivity of 81 (A.U.).

## ASSOCIATED CONTENT

**Supporting Information**. This material is available free of charge via the Internet at http://pubs.acs.org.

## AUTHOR INFORMATION

Corresponding Author

*E-mail: M. Medina-Sánchez (m.medina.sanchez@ifw-dresden.de)

Dr. Bergoi Ibarlucea (bcanton@nano.tu-dresden.de)

Dr. Mariana Medina-Sánchez and Dr. Bergoi Ibarlucea contributed equally to this work

Author Contributions

M.M.S., B.I., L.B., and O.G.S. conceived the project, M.M.S., and B.I designed the experiments with help from N.P., D.D.K., and S.M.W. G.C. and O.G.S. supervised the study. M.M.S. and B.I. performed all experiments. M.M.S. and B.I in close collaboration with N.P., and D. D.K., analyzed the data obtained from the experiments. M.M.S. and B.I. wrote the manuscript. All authors commented on and/or edited the manuscript and figures. All authors have given approval to the final version of the manuscript. Notes The authors declare no competing financial interest.

ACKNOWLEDGMENT

The authors thank to Dr. Cynthia Martínez-Cisneros, Sandra Nestler, Barbara Eichler, Juan Balach, and Lukas Schwarz for technical support. We also thank Dr. Steffen Oswald for the XPS measurements. This work was financed in part via the European Research Council within the European Union's Seventh Framework Programme (FP7/2007-2013)/ERC Grant Agreement No. 306277, the German Excellence Initiative via the Cluster of Excellence EXC 1056 Center for Advancing Electronics Dresden (cfAED) and the DFG Research Unit 1713 "Sensorische Mikro and Nanosysteme".

REFERENCES


(1) Donatin, E.; Drancourt, M. *Médecine Mal. Infect.* **2012**, *42* (10), 453–459.

(2) Neumann, G.; Noda, T.; Kawaoka, Y. *Nature* **2009**, *459* (7249), 931–939.

(3) Van den Brand, J. M. A.; Stittelaar, K. J.; van Amerongen, G.; Rimmelzwaan, G. F.; Simon, J.; de Wit, E.; Munster, V.; Bestebroer, T.; Fouchier, R. A. M.; Kuiken, T.; Osterhaus, A. D. M. E. *J. Infect. Dis.* **2010**, *201* (7), 993–999.

(4) Heid, C. a; Stevens, J.; Livak, K. J.; Williams, P. M. *Genome Res.* **1996**, *6* (10), 986–994.

(5) Karnaushenko, D.; Ibarlucea, B.; Lee, S.; Lin, G.; Baraban, L.; Pregl, S.; Melzer, M.; Makarov, D.; Weber, W. M.; Mikolajick, T.; Schmidt, O. G.; Cuniberti, G. *Adv. Healthc. Mater.* **2015**, *4* (10), 1517–1525.

(6) Thissen, J. B.; McLoughlin, K.; Gardner, S.; Gu, P.; Mabery, S.; Slezak, T.; Jaing, C. *J. Virol. Methods* **2014**, *201*, 73–78.

(7) Drummond, T. G.; Drummond, T. G.; Hill, M. G.; Hill, M. G.; Barton, J. K.; Barton, J. K. *Nat. Biotechnol.* **2003**, *21* (10), 1192–1199.

(8) Bonanni, A.; Pividori, M. I.; del Valle, M. *Analyst* **2010**, *135* (7), 1765–1772.

(9) Zhang, X. Y.; Zhou, L. Y.; Luo, H. Q.; Li, N. B. *Anal. Chim. Acta* **2013**, *776*, 11–16.

(10) Macanovic, A.; Marquette, C.; Polychronakos, C.; Lawrence, M. F. *Nucleic Acids Res.* **2004**, *32* (2), e20.

(11) Berdat, D.; Martin Rodríguez, A. C.; Herrera, F.; Gijs, M. a M. *Lab Chip* **2008**, *8* (2), 302–308.

(12) Santos, A.; Davis, J. J.; Bueno, P. R. *J. Anal. Bioanal. Tech.* **2014**, *S7* (012), 1–15.

(13) Hu, R.; Liu, T.; Zhang, X. B.; Huan, S. Y.; Wu, C.; Fu, T.; Tan, W. *Anal. Chem.* **2014**, *86* (10), 5009–5016.

(14) Wu, C.; Zhou, Y.; Miao, X.; Ling, L. *Analyst* **2011**, *136* (10), 2106–2110.

(15) Lai, S. L.; Chen, C.-H.; Yang, K.-L. *Langmuir* **2011**, *27* (9), 5659–5664.

(16) Li, B.; Yu, Q.; Duan, Y. *Crit. Rev. Biotechnol.* **2013**, *8551*, 1–12.

(17) Yusof, Y.; Yanagimoto, Y.; Uno, S.; Nakazato, K. *World Acad. Sci. Eng. Technol.* **2011**, *49*, 295–299.

(18) Mark, D.; Haeberle, S.; Roth, G.; von Stetten, F.; Zengerle, R. *Chem. Soc. Rev.* **2010**, *39* (3), 1153–1182.

(19) Ben-Yoav, H.; Dykstra, P. H.; Bentley, W. E.; Ghodssi, R. *Biosens. Bioelectron.* **2015**, *64*, 579–585.

(20) Dimaki, M.; Vergani, M.; Heiskanen, A.; Kwasny, D.; Sasso, L.; Carminati, M.; Gerrard, J. A.; Emneus, J.; Svendsen, W. E. *Sensors (Switzerland)* **2014**, *14* (6), 9505–9521.

(21) Riedel, M.; Kartchemnik, J.; Schöning, M. J.; Lisdat, F. *Anal. Chem.* **2014**, *86* (15), 7867–7874.

(22) Benvidi, A.; Tezerjani, M. D.; Jahanbani, S.; Mazloum Ardakani, M.; Moshtaghioun, S. M. *Talanta* **2016**, *147*, 621–627.

(23) Vamvakaki, V.; Chaniotakis, N. A. *Electroanalysis* **2008**, *20* (17), 1845–1850.

(24) Coltro, W. K. T.; Lima, R. S.; Segato, T. P.; Carrilho, E.; de Jesus, D. P.; do Lago, C. L.; da Silva, J. A. F. *Anal. Methods* **2012**, *4* (1), 25–33.

(25) Medina-Sánchez, M.; Miserere, S.; Merkoçi, A. *Lab Chip* **2012**, *12* (11), 1932–1943.

(26) Li, S.; Li, M.; Hui, Y. S.; Cao, W.; Li, W.; Wen, W. *Microfluid. Nanofluidics* **2013**, *14* (3-4), 499–508.

(27) Sugioka, K.; Xu, J.; Wu, D.; Hanada, Y.; Wang, Z.; Cheng, Y.; Midorikawa, K. *Lab Chip* **2014**, *14* (18), 3447–3458.

(28) Lee, C. Y.; Chen, C. M.; Chang, G. L.; Lin, C. H.; Fu, L. M. *Electrophoresis* **2006**, *27* (24), 5043–5050.

(29) Yu, Y.; Chen, J.; Zhou, J. *J. Micromechanics Microengineering* **2014**, *24* (1), 015020.

(30) Schmidt, O. G.; Eberl, K. *Nature* **2001**, *410* (6825), 168.

(31) Harazim, S. M.; Bolaños Quiñones, V. A.; Kiravittaya, S.; Sanchez, S.; Schmidt, O. G. *Lab Chip* **2012**, *12* (15), 2649–2655.

(32) Sharma, R.; Bufon, C. C. B.; Grimm, D.; Sommer, R.; Wollatz, A.; Schadewald, J.; Thurmer, D. J.; Siles, P. F.; Bauer, M.; Schmidt, O. G. *Adv. Energy Mater.* **2014**, *4* (9), 1–8.

(33) Yan, C.; Xi, W.; Si, W.; Deng, J.; Schmidt, O. G. *Adv. Mater.* **2013**, *25* (4), 539–544.

(34) Deng, J.; Ji, H.; Yan, C.; Zhang, J.; Si, W.; Baunack, S.; Oswald, S.; Mei, Y.; Schmidt, O. G. *Angew. Chemie - Int. Ed.* **2013**, *52* (8), 2326–2330.

(35) Karnaushenko, D. D.; Karnaushenko, D.; Makarov, D.; Schmidt, O. G. *NPG Asia Mater.* **2015**, *7* (6), e188.

(36) Grimm, D.; Bof Bufon, C. C.; Deneke, C.; Atkinson, P.; Thurmer, D. J.; Schäffel, F.; Gorantla, S.; Bachmatiuk, A.; Schmidt, O. G. *Nano Lett.* **2013**, *13* (1), 213–218.

(37) Karnaushenko, D.; Münzenrieder, N.; Karnaushenko, D. D.; Koch, B.; Meyer, A. K.; Baunack, S.; Petti, L.; Tröster, G.; Makarov, D.; Schmidt, O. G. *Adv. Mater.* **2015**, *27* (43), 6797–6805.

(38) Martinez-Cisneros, C. S.; Sanchez, S.; Xi, W.; Schmidt, O. G. *Nano Lett.* **2014**, *14* (4), 2219–2224.

(39) Smith, E. J.; Xi, W.; Makarov, D.; Mönch, I.; Harazim, S.; Bolaños Quiñones, V. A.; Schmidt, C. K.; Mei, Y.; Sanchez, S.; Schmidt, O. G. *Lab Chip* **2012**, *12* (11), 1917–1931.

(40) Smith, E. J.; Schulze, S.; Kiravittaya, S.; Mei, Y.; Sanchez, S.; Schmidt, O. G. *Nano Lett.* **2011**, *11* (10), 4037–4042.

(41) Long, G. L.; Winefordner, J. D. *Anal. Chem.* **1983**, *55* (7), 712A – 724A.

(42) Römhildt, L.; Pahlke, C.; Zörgiebel, F.; Braun, H. G.; Opitz, J.; Baraban, L.; Cuniberti, G. *ACS Appl. Mater. Interfaces* **2013**, *5* (22), 12029–12035.

(43) Chrisey, L. a; Lee, G. U.; O'Ferrall, C. E. *Nucleic Acids Res.* **1996**, *24* (15), 3031–3039.

(44) Taylor, S. R. *IEEE Trans. Electr. Insul.* **1989**, *24* (5), 787–806.

(45) Ma, W.; Kuang, H.; Xu, L.; Ding, L.; Xu, C.; Wang, L.; Kotov, N. A. *Nat. Commun.* **2013**, *4*, 1–8.

(46) Wu, W.; Kirimli, C. E.; Shih, W. H.; Shih, W. Y. *Biosens. Bioelectron.* **2013**, *43* (1), 391–399.

(47) Cui, H.-F.; Xu, T.-B.; Sun, Y.-L.; Zhou, A.-W.; Cui, Y.-H.; Liu, W.; Luong, J. H. T. *Anal. Chem.* **2015**, *87* (2), 1358–1365.

(48) Kong, R.-M.; Song, Z.-L.; Meng, H.-M.; Zhang, X.-B.; Shen, G.-L.; Yu, R.-Q. *Biosens. Bioelectron.* **2014**, *54*, 442–447.

(49) Gu, H.; Su, X. di; Loh, K. P. *J. Phys. Chem. B* **2005**, *109* (28), 13611–13618.

(50) Bizid, S.; Mlika, R.; Haj Said, A.; Chemli, M.; Korri Youssoufi, H. *Sensors Actuators B Chem.* **2016**, *226*, 370–380.

(51) Yang, L.; Li, X.; Li, X.; Yan, S.; Ren, Y.; Wang, M.; Liu, P.; Dong, Y.; Zhang, C. *Anal. Biochem.* **2016**, *492*, 56–62.

(52) Yang, T.; Meng, L.; Chen, H.; Luo, S.; Li, W.; Jiao, K. *Adv. Mater. Interfaces* **2016**, *3* (7), doi:10.1002/admi.201500700.

(53) Wang, C.; Yuan, X.; Liu, X.; Gao, Q.; Qi, H.; Zhang, C. *Anal. Chim. Acta* **2013**, *799*, 36–43.

(54) Zhang, W. *J. Solid State Electrochem.* **2015**, *20* (2), 499–506.

(55) Benvidi, A.; Rajabzadeh, N.; Molaye Zahedi, H.; Mazloum-Ardakani, M.; Heidari, M. M.; Hosseinzadeh, L. *Talanta* **2015**, *137*, 80–86.

(56) Engstrom, R.; Weber, M. *Anal. Chem.* **1986**, *58* (4), 844–848.

(57) Bixon, M.; Giese, B.; Wessely, S.; Langenbacher, T.; Michel-Beyerle, M. E. E.; Jortner, J. *Proc. Natl. Acad. Sci. U. S. A.* **1999**, *96* (21), 11713–11716.

(58) Klotsa, D.; Römer, R. R. A.; Turner, M. M. S. *Biophys. J.* **2005**, *89* (4), 2187–2198.

(59) Xiang, L.; Palma, J. L.; Bruot, C.; Mujica, V.; Ratner, M. a; Tao, N. *Nat. Chem.* **2015**, *7* (3), 221–226.

(60) Hu, Y.; Li, F.; Bai, X.; Li, D.; Hua, S.; Wang, K.; Niu, L. *Chem. Commun. (Camb).* **2011**, *47* (6), 1743–1745.

(61) Kelley, S. O.; Jackson, N. M.; Hill, M. G.; Barton, J. K. *Angew. Chemie - Int. Ed.* **1999**, *38* (7), 941–945.

(62) Endres, R. G.; Cox, D. L.; Singh, R. R. P. *Rev. Mod. Phys.* **2004**, *76* (1), 195–214.

(63) Ramos, M. M. D.; Correia, H. M. G. *Nanotechnology* **2008**, *19* (37), 375202.

(64) Li, C.-Y.; Hemmig, E. A.; Kong, J.; Yoo, J.; Hernández-Ainsa, S.; Keyser, U. F.; Aksimentiev, A. *ACS Nano* **2015**, *9* (2), 1420–1433.

(65) Slinker, J. D.; Muren, N. B.; Renfrew, S. E.; Barton, J. K. *Nat. Chem.* **2011**, *3* (3), 228–233.

(66) Balducci, A.; Doyle, P. S. *Macromolecules* **2008**, *41* (14), 5485–5492.

(67) Tang, J.; Du, N.; Doyle, P. S. *Proc. Natl. Acad. Sci.* **2011**, *108* (25), 16153–16158.

(68) Duffy, D. C.; McDonald, J. C.; Schueller, O. J. A.; Whitesides, G. M. *Anal. Chem.* **1998**, *70* (23), 4974–4984.

(69) Hinterwirth, H.; Kappel, S.; Waitz, T.; Prohaska, T.; Lindner, W.; Lämmerhofer, M. *ACS Nano* **2013**, *7* (2), 1129–1136.

(70) Staros, J. V.; Wright, R. W.; Swingle, D. M. *Anal. Biochem.* **1986**, *156* (1), 220–222.

(71) Kick, A.; Bönsch, M.; Katzschner, B.; Voigt, J.; Herr, A.; Brabetz, W.; Jung, M.; Sonntag, F.; Klotzbach, U.; Danz, N.; Howitz, S.; Mertig, M. *Biosens. Bioelectron.* **2010**, *26* (4), 1543–1547.

(72) Owczarzy, R.; Moreira, B. G.; You, Y.; Behlke, M. A.; Walder, J. A. *Biochemistry* **2008**, *47* (19), 5336–5353.

(73) Nadal, P.; Pinto, A.; Svobodova, M.; Canela, N.; O'Sullivan, C. K. *PLoS One* **2012**, *7* (4), e35253.

TOC figure

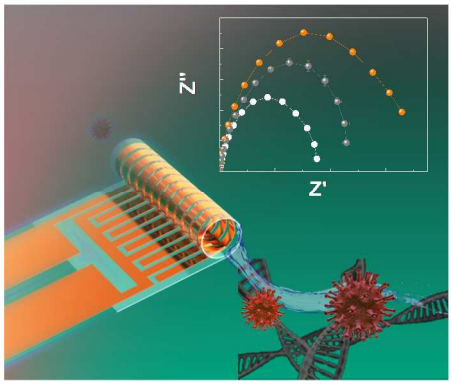


**Synopsis**

A highly sensitive label-free DNA biosensor is presented. It involves the fabrication of interdigitated microelectrodes with a rolled-up configuration inside a microchannel. These biosensors show four-fold improved detection ability compared to equivalent planar electrodes, and more reproducible behavior. Attomolar level detection of Avian Influenza Virus H1N1 DNA is achieved. The effect of the rolled-up configuration for the greatly enhanced detection is analyzed by using a model fit analysis as well as electric field calculation.